

Project Daedalus

Tejas Vinod, Erika L Ashley, Seokhyeon Byun, Julian Drake, Timothy McEvoy, David Ward, Dora Naz Erdogan, Steven H Meadows, Jay Sabharwal, Larsen VanOfferen, * and Dr. Kevin A Shinpaugh †
Virginia Polytechnic Institute and State University, Blacksburg, VA, 24061

Project Daedalus is an unmanned space mission with the objective of autonomously performing a chain of three or more operations to demonstrate an ISAM capability. The mission is required to launch by the end of the decade. The payload must be designed to conform to the BCT X-Sat Venus class bus mass, volume, and power constraints. The Project Daedalus payload is designed to additively manufacture metal parts and laser weld the manufactured parts into a larger piece. The payload will use Directed Acoustic Energy Deposition to overcome the harsh power and volume constraints of a SmallSat bus. The payload will operate autonomously with limited remote commands with an AI non-destructive evaluation system to monitor the additive manufacturing process. Project Daedalus is expected to launch before 2030 and complete its mission within two years in low Earth orbit. The program cost is estimated at approximately \$50.4 million. This paper provides the decision making and technical information of the conceptual payload design for Project Daedalus.

I. Introduction

The Daedalus mission is designed to achieve the goals of the COSMIC Capstone Challenge (C3). The prompt for the challenge is to "design a payload, to be hosted about the BCT X-Sat Venus Class bus, that will demonstrate a chain of three or more operations that provide an on-orbit, autonomous ISAM capability" [1]. The team was provided resources to determine what past In-Space Servicing, Assembly and Manufacturing (ISAM) missions have pushed the boundaries of what is possible in space. Among these documents the 2024 edition of the ISAM State of Play published by NASA summarizes the capability areas and scientific achievements from previous missions [2]. The eleven functional capabilities under in-space assembly and manufacturing are:

- 1) Robotic Manipulation
- 2) RPO, Capture, Docking, and Mating
- 3) Relocation
- 4) Planned Repair, Upgrade, Maintenance, and Installation
- 5) Unplanned or Legacy Repair and Maintenance
- 6) Refueling and Fluid Transfer
- 7) Structural Manufacturing and Assembly
- 8) Recycling, Reuse, and Repurposing
- 9) Parts and Goods Manufacturing
- 10) Surface Infrastructure
- 11) Inspection and Metrology

The team derived top-level system requirements from the Request for Proposal (RFP) provided by the COSMIC Capstone Challenge. These mission requirements are shown in Table 1. A comprehensive table including each system requirement is located in Appendix A.

Demonstrating the functional capabilities identified by the ISAM State of Play in space requires unique spacecraft systems. With the mission confined to the BCT – X-Sat Venus class bus, the team selected structural manufacturing and assembly as the focus of the project.

Project Daedalus is focused on in-space additive manufacturing and assembly. This decision was made after considering the current and future technical impacts of in-space additive manufacturing. The ability to fabricate and assemble structures on-orbit with compact feedstock materials would be a step towards overcoming many launch limitations of modern space missions. Currently a payload must be capable of standing under its own weight, it must fit within the payload volume of its launch vehicle, and its mass must not exceed the launch vehicle's limits. Overcoming

*Undergraduate Students, Kevin T. Crofton Department Of Aerospace And Ocean Engineering, 1600 Innovation Drive Blacksburg, VA 24061.

†Collegiate Professor and Faculty Advisor, Kevin T. Crofton Department Of Aerospace And Ocean Engineering, 1600 Innovation Drive Blacksburg, VA 24061. Associate Fellow AIAA.

Table 1 Mission Requirements. The mission requirements derived from the RFP provide mission objective and constraints for Project Daedalus. A detailed table with requirements derived from other sources is located in Appendix A.

Req ID	Requirement	Source
SYS1.0	The system shall perform three or more operations to demonstrate an on-orbit ISAM capability.	RFP [1]
SYS2.0	The system shall operate autonomously with limited remote commands.	RFP [1]
SYS3.0	The system shall meet the BCT X-Sat Venus Class bus specifications.	RFP [1]
SYS4.0	The system shall utilize power generated by the BCT-X Sat Venus class bus.	RFP [1]
SYS9.0	The system shall launch before 2030.	RFP [1]

these limits would revolutionize the design of large space systems such as space stations and habitats. By demonstrating the ability to manufacture and assemble structure-like components autonomously while in Earth orbit, Project Daedalus seeks to add novel research to the structural manufacturing and assembly ISAM capability.

Research was done on current commercial additive manufacturing techniques [3], experimental additive manufacturing technologies [4–7], and their applications in space [8–13]. Following trade studies to determine the optimal additive manufacturing system for the mission, Directed Acoustic Energy Deposition (DAED) with Aluminum 6061 feedstock was chosen. The mission scope includes assembly of multiple components which drove the selection of a laser welding system to fuse printed pieces together as an additional demonstration of on-orbit assembly capabilities.

To accomplish the goals provided by the COSMIC Capstone Challenge, the team developed and modeled a conceptual payload. The core subsystems and operation of this payload are discussed in Section II.

A Concept of Operations (ConOps) for Project Daedalus is shown in Figure 1. Key operations during the satellite’s lifecycle are shown. These events include launch and deployment, specimen fabrication, specimen assembly, non-destructive specimen evaluation, and satellite de-orbit. Project Daedalus is scheduled to launch by 2030 and deorbit by 2032.

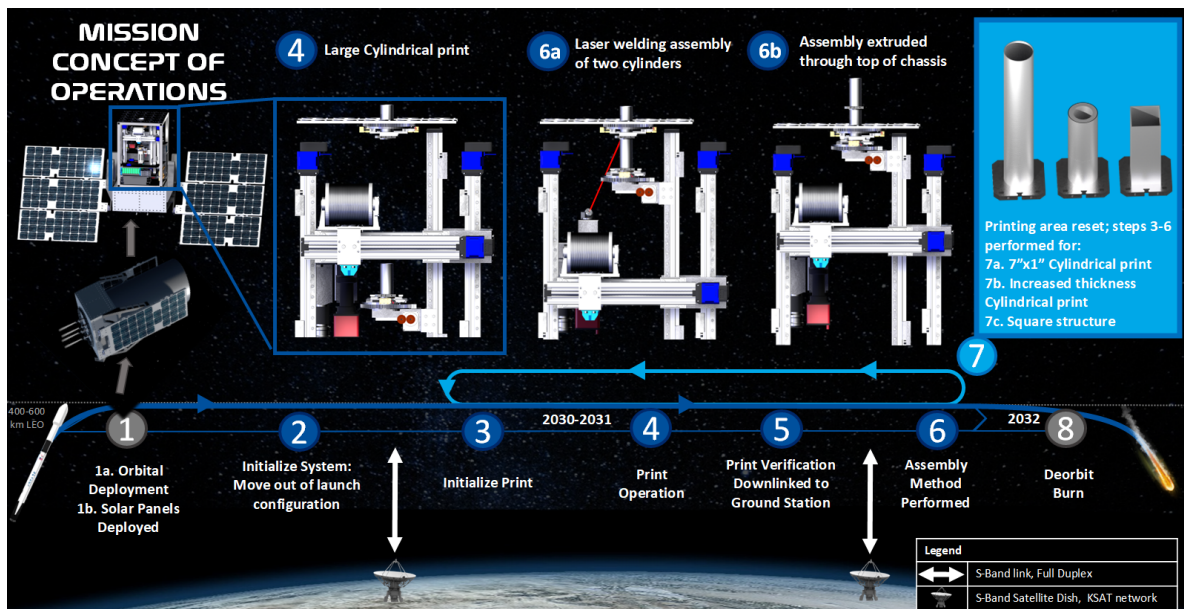


Fig. 1 Project Daedalus Concept of Operations. The ConOps for Project Daedalus details the operations the payload will perform after deployment and the satellite life cycle. Following launch, the payload will be initialized and checked for deformations. The payload will then additively manufacture a specimen. The additively manufactured specimen will be assembled with other specimens and the process will repeat.

II. Mission Design

A. Payload Overview

The design of the payload for Project Daedalus is separated into multiple core subsystems. The core mechanical subsystems and their operations are shown in Figure 2. A list of the core subsystems and their purpose are provided in Table 2.

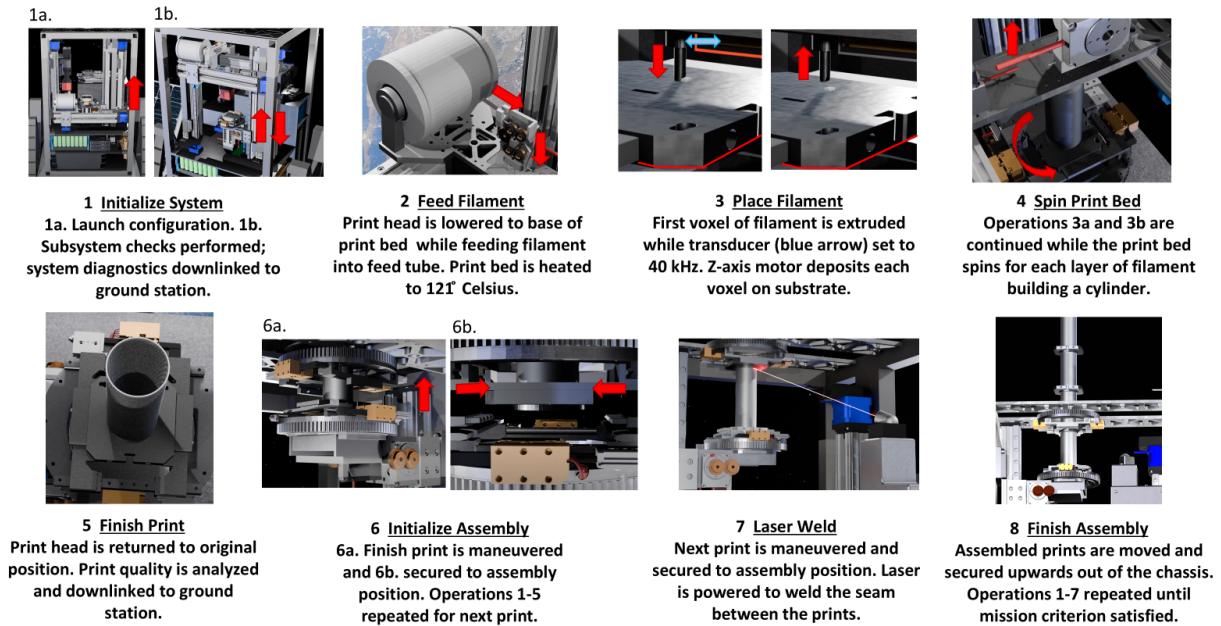


Fig. 2 Payload Concept of Operations. The general operations in the printing process are shown in steps 2-5. The finished print is then moved to the top of the chassis and secured until the next print is manufactured. The prints are welded together by a laser mounted to the side of the chassis and spinning of the print bed. These steps repeat until all of the substrates are used or mission criteria achieved.

Table 2 Payload Subsystems. The payload is comprised of five main systems. Each system is divided into subsystems with a purpose defined in the table below. The fabrication and AI monitoring systems are unique to Project Daedalus.

System	Subsystem	Purpose
Fabrication	Deposition	Deposit Aluminum 6061 with acoustic softening.
	Traversal	Move the deposition subsystem and rotating print bed.
	Assembly	Maneuver finished and failed parts and weld finished parts together.
AI Monitoring	AI NDE System	Active monitoring and control of the fabrication system.
	Optical Cameras	Provide optical data to AI NDE system.
	IR Cameras	Provide infrared data to AI NDE system.
Data Handling	Core Computer	Control of key spacecraft systems and communication with the bus computer.
	Data Storage	Store diagnostic and mission information to transmit to ground station.
Power	PCDU	Distribute power to payload systems.
	Battery	Provide additional power storage.
Thermal	Active Cooling	Remove heat from deposition and assembly systems.

The interactions between the payload systems are shown in the system block diagram (Figure 3). The system

block diagram shows the identified satellite bus systems and their interactions with the payload systems. The primary interactions between the payload and satellite bus are power supplied to the payload from the satellite bus power generation system and data transmission from the payload through the satellite bus communication system.

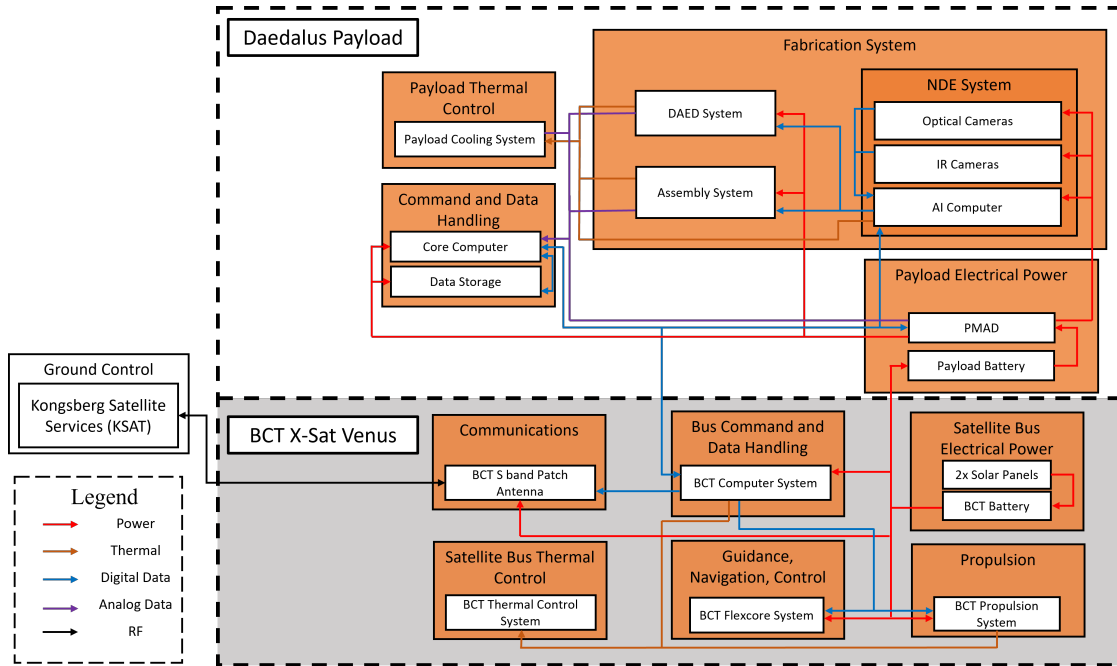


Fig. 3 System Block Diagram. This diagram illustrates the high-level architecture of the payload system, showcasing the major subsystems and their interconnections. The blocks represent different subsystems, and the arrows indicate the flow of information, thermal energy, or power between them.

B. BCT Overview

The Blue Canyon Technologies Venus Class satellite bus is the selected platform for this mission. The payload utilizes the dual-bank solar configuration of the Venus class, increasing the available solar array power at the expense of payload volume. The specifications of the chosen configuration and orbital regime are listed in Table 3. Due to limited information from Blue Canyon Technologies, this specification does not include the propulsion system used for the mission, which affects the final wet mass value.

Table 3 BCT Venus Class Bus Specifications.

Specification	Value	Source
Bus Class	ESPA-Standard or larger, 15" launch vehicle interface	[14]
Pointing Accuracy	$\pm 0.002^\circ$ (1-sigma), 3 axes, 2 Trackers	[14]
Slew Rate	> 1.5 degrees per second	[15]
Solar Array Power	444 Watts (two-panel configuration)	[14]
Payload Power	60 Watts	[15]
Energy Storage	13.6 Amp-hours	[14]
Payload Volume	17.0 x 16.4 x 27.0 inches	[14]
Orbit Lifetime	>5 Years in LEO	[14]
Max Payload Mass	78 kg	[15]
Bus Dry Mass	64 kg	[15]

C. Design Requirements

The subsystems in the payload for Project Daedalus are required to successfully complete the mission. Requirements for each subsystem were generated to achieve this goal. The requirements for each payload subsystem are in Table 4.

Table 4 Payload Subsystem Requirements. The payload subsystem requirements are derived from the top level system requirements. These include requirements for the fabrication system, AI monitoring system, and power system. Requirements were derived from design decisions or from additional documentation.

Req ID	Requirement	Source
SYS1.0	The system shall perform three or more operations to demonstrate an on-orbit ISAM capability.	RFP [1]
AM1.1	The system shall additively manufacture a specimen.	Derived
ASM1.1	The system shall assemble additively manufactured specimens together	Derived
ASM1.2	The system shall laser weld the specimens together	Derived
SYS2.0	The system shall operate autonomously with limited remote commands.	RFP [1]
AI2.1	The system shall utilize an on-board AI computer to control, inspect, and monitor the additive manufacturing system.	Derived
AI2.2	The AI computer shall control all printing operations during additive manufacturing, including initiation execution, and shutdown of print sequences.	Derived
SYS4.0	The system shall utilize power generated by the BCT-X Sat Venus class bus.	RFP [1]
POW4.1	The system shall use a power bus of 28 V DC	BCT Documentation [15]
POW4.2	The system shall have onboard energy storage of 38.8 Ah	Derived
POW4.3	The system shall provide 60 W of power to the payload in full sun exposure	BCT Documentation [15]

D. Orbit Architecture and Launch Considerations

The payload will be launched using the SpaceX Bandwagon rideshare program [16]. The estimated cost of this launch is \$1.3 million. The orbit resulting from this launch option is low Earth orbit (LEO) at an altitude between 400 – 600 km and an inclination of 45°. A simulation in Ansys Systems Toolkit (STK) [17] was performed. Initial conditions were a circular orbit at 45° inclination at an initial altitude of 550 km and launch from Cape Canaveral launch site at 28°N, –81°W. The simulation was performed over the date range of March 22, 2030 to March 22, 2032. The data collected was the total ionizing dose (TID) the payload experiences for the mission, the solar exposure of the payload each orbit cycle, and the average temperature over an orbit period.

The TID for the mission assuming 2 mm of shielding was 1600 rad-s. An estimate of the total solar exposure was recorded for use in determining the power budget of the payload. The average temperature over an orbit period was found to be between –40°C to –90°C. The simulation results are shown in Appendix B.

E. Fabrication System

The fabrication system of the payload is made up of three subsystems: the deposition subsystem, the traversal subsystem, and the assembly subsystem. Each of these subsystems will be discussed in-depth in this section. The child requirements for the fabrication system are shown in Table 5.

Table 5 Fabrication System Requirements. The fabrication system requirements include requirements for the additive manufacturing subsystem as well as the assembly subsystem. These requirements further specify the additive manufacturing and assembly process.

Req ID	Requirement	Source
SYS1.0	The system shall perform three or more operations to demonstrate an on-orbit ISAM capability.	RFP [1]
AM1.1	The system shall additively manufacture a specimen.	Derived
AM1.1.1	The system shall use the Directed Acoustic Energy Deposition process.	Trade Study
AM1.1.2	The system shall use Al-6061 feedstock.	Trade Study
AM1.1.3	The system shall excite the print deposition head to 60 kHz.	Derived
AM1.1.4	The system shall apply a nominal force of 100 Newtons on the feedstock material.	Derived
AM1.2	The system shall operate on a traversal system with a rotational and axial axis.	Derived
ASM1.1	The system shall assemble additively manufactured specimens together.	Derived
ASM1.1.1	The system shall laser weld the specimens together.	Derived
ASM1.2	The system should add minimal mechanical complexity.	Derived

1. Deposition System

The additive manufacturing system of the payload is a Directed Acoustic Energy Deposition (DAED) system. This system was selected through a trade study of additive manufacturing technologies. Directed acoustic energy deposition is an experimental technique of additive manufacturing. Currently the primary source of research on this technology is a research group at Arizona State University [5–7]. A patent for the deposition technology enabling this additive manufacturing technique is held by Dr. Keng Hsu and Dr. Anagh Deshpande, the primary researchers in recent journal articles on this process [4]. Their works were used in our trade study to compare DAED with other potential additive manufacturing candidates. The trade study comparing the feasible additive manufacturing processes for the mission is in Appendix C.

The core deposition process in the payload involves vibrating the deposition head at a specified frequency and applying a force to compress material deposited through the deposition head into a voxel on the build area. The parameters for the Arizona State experimental DAED machine are a deposition head vibration frequency of 60 kHz and a deposition head shear displacement of 1.1 μm . These were found to be the optimal parameters for manufacturing with Aluminum 6061. A model of this DAED deposition system is shown in Figure 4.

Aluminum 6061 was chosen as the feedstock material for the deposition system. This decision was made following a trade study of metals commonly used for aerospace purposes. This trade study is located in Appendix C. The machine will use a vibrational frequency of 60 kHz, a vibrational amplitude of 1.1 μm , and apply a nominal force of 100 N to the aluminum feedstock. These values were derived from research on directed acoustic energy deposition with Aluminum 6061 by the Arizona State University research group.

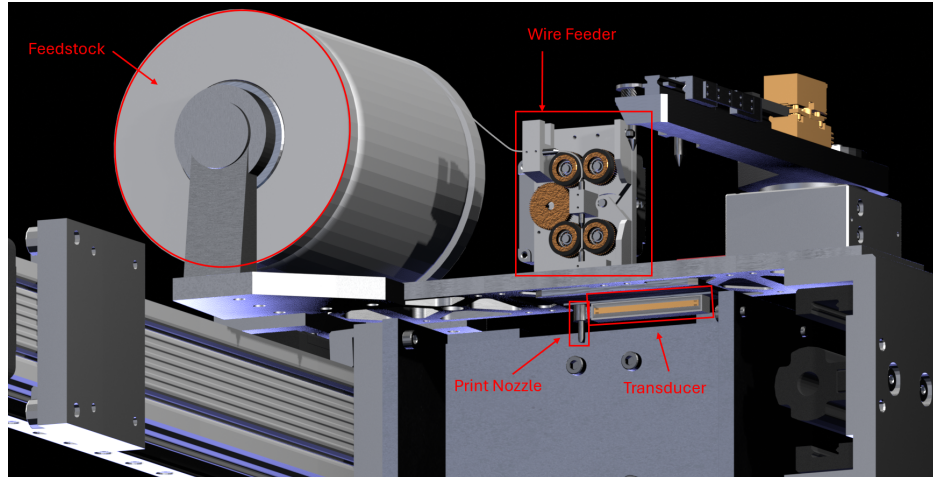


Fig. 4 Deposition System Schematic. The deposition system includes a feedstock management system and the deposition head connected to a piezoelectric transducer. A pinch roller system feeds the Al-6061 wire feedstock through the deposition head. The deposition head is vibrated at 60 kHz and pressed into the deposited material with a nominal force of 100 N to compress the material into a voxel on the build area.

2. Traversal System

The traversal subsystem is oriented with two transverse axes and a rotational axis. Three degrees of freedom for the deposition system are required to additively manufacture with directed acoustic energy deposition. The three axes of motion for the traversal system are the X -axis, Θ -axis, and Z -axis. These axes are shown on the model in Figure 5. The feedstock storage reel has been removed from the model for clarity.

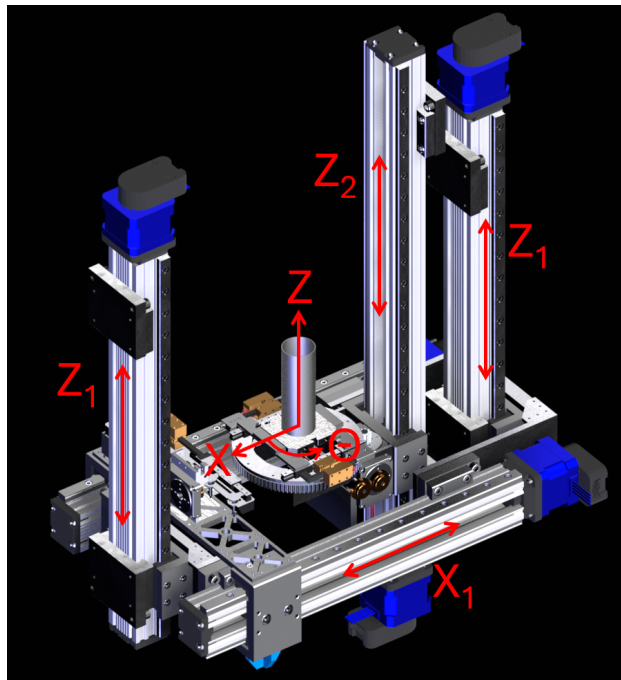


Fig. 5 Traversal System Schematic. This figure shows the traversal system of the payload. The axes of motion are shown in the build volume. The traversal system moves the deposition head and build substrates to allow the deposition system to additively manufacture specimens. Note that the feedstock storage system is removed for clarity on the traversal system.

The three axis traversal system is used to move the point at which the deposition system deposits its aluminum feedstock. The X -axis is the axis by which the deposition head is translated radially relative to the build plate. This radial translation is required to allow the system to build a structure with integrity. Without this axis the system can only manufacture cylinders with one voxel width of thickness. Motion on this axis is performed with two NEMA 23-31-01PD-AMT112S stepper motors [18].

The Z -axis translates the deposition head vertically relative the the build plate. The directed acoustic energy deposition manufacturing process requires a nominal force of 100 N in the Z_1 -axis direction to operate. Two NEMA 23-31-01PD-AMT112S stepper motors were selected to control this motion [19]. This axis is also used for vertical translation of the printing bed. The actuator for this motion is shown as Z_2 in the Figure above.

The Θ axis in Figure 5 is the axis by which the deposition point on the build plate is moved. A rotational axis was chosen due to the additional symmetry to the deposition system it provides compared to a traditional linear three axis additive manufacturing traversal system. The motion of this axis is performed with a NEMA 11-20-02D-AMT112S stepper motor [20].

The rotational plate of the traversal system houses multiple independent substrates. Options for removing built materials from the build plate of the additive manufacturing system were considered. These options included cutting the base of the manufactured specimen to remove it, utilizing a different thermal properties to naturally separate the specimen from the material, and replaceable substrates. Following qualitative analysis on these three methods it was found that sawing a specimen would be both mechanically complex and introduce unnecessary risks. Removing a specimen with different thermal properties was not demonstrated to be feasible for specimens manufactured with the directed acoustic energy deposition process. By pairwise comparison a consumable substrate is the best available option to enable repeated additive manufacturing. A model of the substrate is shown in Figure 6.

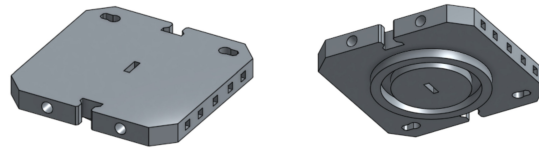


Fig. 6 Substrate Model. The substrate used by the fabrication subsystem of the Daedalus payload is a rectangular plate with anchor points designed to be manipulated by the traversal and assembly systems. Substrates are stored within the traversal system and replaced when a new specimen must be fabricated.

The substrates used by the fabrication system are designed to lock into the rotating build plate. The deposition system then deposits aluminum onto the substrate. In the event that the fabrication process fails, the substrate can be removed with the failed specimen and placed into a storage compartment in the payload.

3. Assembly System

The assembly system is designed to maneuver a finished specimen away from the build area and laser weld two specimens together. This is done by directly gripping the specimen and translating it in the positive Z direction using a NEMA 23-31-01PD-AMT112S stepper motor [18]. The substrate is locked in place above the additive manufacturing system.

Upon completion of another specimen, the second specimen is aligned with the first specimen. A YLM-150/1500-QCW laser modified for space use is used to weld the specimens together [?]. The top of the second specimen is welded with the bottom of the substrate of the first specimen. The assembly subsystem is shown in Figure 7.

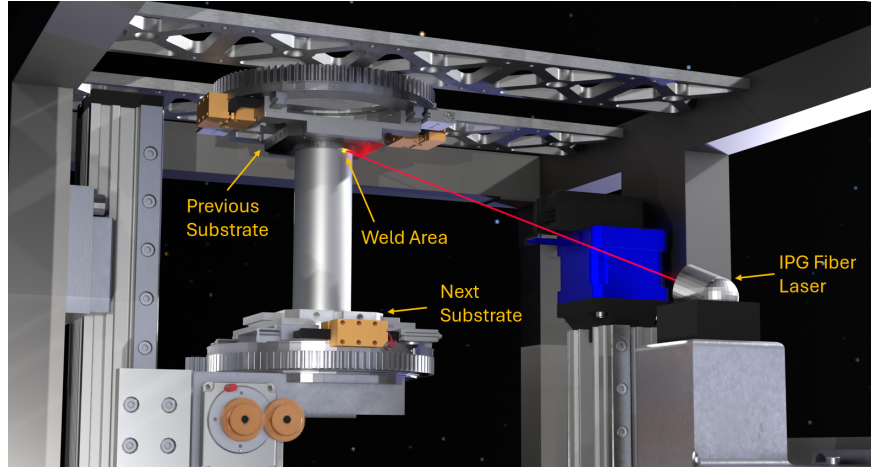


Fig. 7 Assembly System Schematic. Fabricated specimen are translated in the Z-direction to be joined with the substrate in place above them. Laser welding is used to join the specimen to the substrate it contacts.

F. Monitoring & Inspection Methodology

Monitoring and inspection on the payload is divided into two parts. An AI controlled Nondestructive Evaluation (NDE) system actively monitors and corrects fabricated specimens during the additive manufacturing process. A core payload computer monitors other payload systems and resolves errors following Fault Detection, Isolation, and Recovery (FDIR) protocols.

1. Non-Destructive Evaluation

The AI NDE system requirements are shown in Table 6. These include requirements for the AI system and the camera systems used in the non-destructive evaluation of fabricated specimens.

The most common NDE methods for AM in space traditionally involve around ultrasound and thermography. These methods rely on specialized, high-cost equipment optimized for space conditions. This equipment often under-performs compared to commercially available technologies on Earth due to constraints imposed by custom-designed components for the space environment [22]. Adapting Commercial Off The Shelf (COTS) electronics with radiation shielding for in-space use will reduce development costs and timelines for Project Daedalus. The payload will incorporate optical inspection techniques with high-performance COTS electronics and a Convolutional Neural Network (CNN).

The different machine learning systems under consideration for the NDE algorithm for the fabrication system are in-situ three-dimensional digital image correlation (3D-DIC) [23], machine vision-based detection of surface defects using PointNet [24], and Spatio-temporal 3D object detection with YOLO4D models [25].

An AI system was selected for the NDE system because traditional image processing techniques are limited in flexibility and scalability. In contrast, CNNs provide powerful spatial feature extraction capabilities. This enables accurate identification of surface anomalies and defect patterns within complex printed geometries. CNNs have been demonstrated to outperform traditional algorithms in image-based defect classification due to their ability to automatically learn multi-level visual representations from raw pixel data [26].

Training a CNN from scratch requires extensive labeled data and computational resources. These are constrained in the early stages of mission development and on-orbit operations. To address this, transfer learning with CNNs can be used to increase the speed at which a neural network is trained. Transfer learning leverages pre-trained CNN models initially developed on large-scale datasets [27]. These models can be fine-tuned on Earth-based DAED image datasets generated under controlled terrestrial conditions using the same manufacturing process planned for orbit.

The effectiveness of this approach is supported by Patil et al. [28], who demonstrated that the VGG16 CNN could achieve a classification accuracy of 94.7% across defect categories after it was fine-tuned with a dataset of directed energy deposition products. Yang et al. validated the adaptability of transfer learning for additive manufacturing inspection [29]. Their research showed that surface defects could be robustly identified under varying geometric and visual conditions.

The AI-onboard computer was selected with the trade study shown in Appendix D. System constraints such as power

Table 6 Artificial Intelligence Requirements. This table displays the artificial intelligence requirements along with optical and infrared camera requirements as derived from the RFP and other sources.

Req ID	Requirement	Source
SYS2.0	The system shall operate autonomously with limited remote commands.	RFP [1]
AI2.1	The AI computer shall control all printing operations during additive manufacturing, including initiation execution, and shutdown of print sequences.	Derived
AI2.2	The AI computer shall control all printing operations during additive manufacturing, including initiation execution, and shutdown of print sequences.	Derived
AI2.3	The AI computer shall inspect printed parts using real-time visual data to detect defects or anomalies during manufacturing.	Derived
AI2.4	The AI computer shall analyze fault indicators and system health data to autonomously change the operational status of the additive manufacturing system.	Space Trusted Autonomy Readiness Levels[21]
CAM2.3.1.1	The optical camera shall be of resolution of 5MP or greater.	Derived
CAM2.3.1.2	The optical camera shall communicate over the MIPI-CSI protocol and connector.	Derived
CAM2.3.1.3	The IR camera shall have the wavelength range of 7.5-13 μm in order to successfully perform thermal imaging.	Derived
CAM2.3.1.4	The IR camera shall be optimized for short-range thermal imaging at distances ranging from 5 cm to 20 cm.	Derived

availability, volume, radiation tolerance, and overall inspection performance were used to compare different commercial AI computers. The selected AI computer was the NVIDIA Jetson Xavier NX.

Optical and infrared cameras were chosen as the sensors to provide data to the NDE system. Optical camera selection was driven by the need for high-resolution, low-power imaging suitable for surface-level defect recognition. The Arducam IMX219 meets the camera requirements for the NDE system and was selected. It has a 3280 x 2464 resolution with a power draw of 1.0 W [30]. This configuration enables reliable visual image-based CNN inspection while maintaining compatibility payload and power budget.

Infrared inspection of additive manufacturing with thermal imaging based failure detection has been proven effective for Earth-based AM systems [31, 32]. This inspection process will be used by the NDE system along with the optical cameras. The FLIR Boson+ infrared camera was selected. The Boson+ has a 320 x 256 pixel resolution, 50 degree field of view, and a consumption of 0.5 W [33].

The NVIDIA Jetson is not space rated as a COTS component. The risk of a Single Event Effect (SEE) compromising the AI computer system is high without proper radiation protection [34, 35]. Options for radiation shielding include experimental Plasteel shielding [36] and conventional aluminum shielding. Aluminum shielding was selected as radiation shielding for the AI computer system due to its validation in space flight. Following TID analysis in STK, a 2 mm thick aluminum radiation shield is required to reduce the risk of damage from radiation to acceptable levels.

2. Fault Detection, Isolation, and Recovery

The core payload computer is responsible for autonomously monitoring payload health. It will utilize a Fault Detection, Isolation, and Recovery (FDIR) system inspired by NASA's High Performance Spaceflight Computing (HPSC) initiative [37]. The architecture emphasizes computational robustness, autonomous error handling, and mission resilience. Following a hierarchical FDIR framework enables detection and recovery from unit-level to full system-level faults. The core computer will continuously receives telemetry and status data from all major payload subsystems.

The FDIR system will receive temperature readings and fault status indicators from the mechanical and computer components in the fabrication system. It will also monitor the voltage, current, and internal temperature of the payload power system as well as the status of the active and passive payload thermal systems.

The FDIR process operates through four sequential stages:

- 1) **Fault Detection:** Real-time monitoring of all telemetry streams for deviations, signal dropouts, or out-of-range values.
- 2) **Fault Isolation:** Identification of the affected subsystem, activation of safe mode, engagement of redundant components (if available), and request for additional diagnostics.
- 3) **Fault Identification:** Classification of the fault into severity levels:
 - Level 0: Minor, single unexpected data point
 - Level 1: Subsystem non-responsiveness
 - Level 2: Multiple inconsistent or anomalous values
 - Level 3: Failure within the FDIR handling process itself
 - Level 4: Critical or cascading faults affecting system-level functionality
- 4) **System Reconfiguration:** Dispatch of corrective commands (e.g. reboot, reinitialize). If unsuccessful, the system shifts to backup hardware. Persistent unresolved faults result in a downlink of diagnostic data to ground operations for human intervention.

This structured and hierarchical FDIR implementation ensures that the payload system can respond autonomously to the anomalies with minimal ground intervention [38]. Figure 8 shows this process in a flowchart.

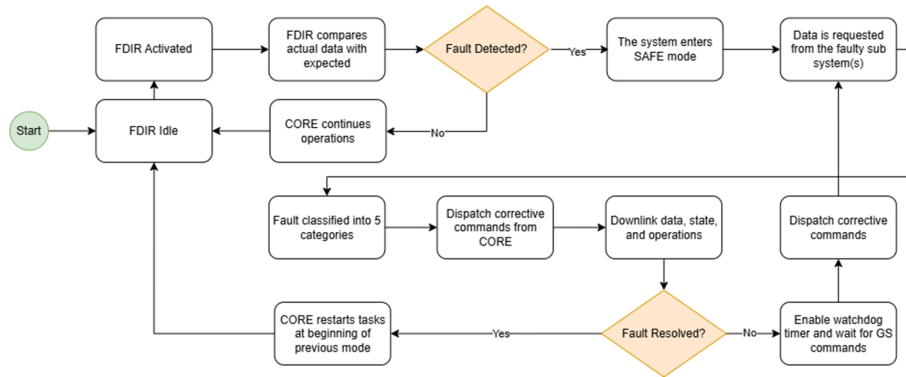


Fig. 8 Fault Detection, Isolation, and Recovery (FDIR) system flowchart The FDIR system will monitor the payload until a fault is detected. The system will then enter safe mode and the FDIR system will classify the fault and attempt to resolve the error. The FDIR system will contact ground operations and if it is unable to resolve the error on its own the ground team can attempt to recover the system.

G. Power System

The 13.2 Ah of energy storage provided by the BCT X-Sat Venus class bus is not sufficient for the payload. Additional battery modules produced by Blue Canyon Technologies were added to the payload space to increase the total energy storage while maintaining the original 28 volts of the system. The power requirements for the payload system are shown in Table 7.

Table 7 Power Requirements. The power requirements for the payload are derived from the RFP and supporting documentation for the BCT X-Sat Venus class bus. Conflicting documentation on the specifications of the spacecraft bus resulted in the assumption that the nominal power generation of the bus is 60 Watts.

Req ID	Requirement	Source
SYS4.0	The system shall utilize power generated by the BCT-X Sat Venus class bus.	RFP [1]
POW4.1	The system shall use a power bus of 28 V DC.	BCT Documentation [15]
POW4.2	The system shall have onboard energy storage of 38.8 Ah	Derived
POW4.2.1	The system should lose no less than 2% battery charge per cycle in hibernation.	Derived
POW4.3	The system shall provide 60 W of power to the payload in full sun exposure.	BCT Documentation [15]

1. System Components

The specifications for each payload power component are listed in Appendix F. The payload contains a 16P8S (16 parallel, 8 series) battery configuration in the form of eight 2P8S battery modules. This configuration of MJ1 18650 batteries provides 28 Volts and 25.2 Amp-hours of additional energy storage [39].

The STARBUCK-MICRO power conditioning and distribution unit (PCDU) manages power between the electronic systems in the payload and satellite bus. This includes an array of sensors that will send telemetry to the core computer modules for health monitoring and FDIR responses. It will assess specific battery modules from its on board controller and is powered by a separate 160 Wh Lithium-ion battery [40]. The PMAD has a Design life of 5 years in LEO and is rated for 20 kRAD. This exceeds both the maximum duration and radiation dose of the 2 year long mission. Simulation data provided in Appendix B was used as an estimate of the radiation dose across the entire mission.

The dual solar arrays located on the sides of the BCT Venus class bus provide 60 W nominally to the payload at 30% efficiency in direct sunlight [15].

2. Power Cycling

In order to ensure mission success, a model was constructed to simulate the energy storage and power cycles needed to complete a print, shown in Figure 9. The usable region of battery charge is between 20% and 80%, leaving a safety margin of charge at the lowest power. This extends the usable lifespan of the batteries by not fully charging. Figure 9 also shows the estimated time to complete a the 3 inch tall standard print. The print time of 100 hours, or 63 orbital cycles, means that all mission objectives are reasonably achievable within the 2 year mission timeline.

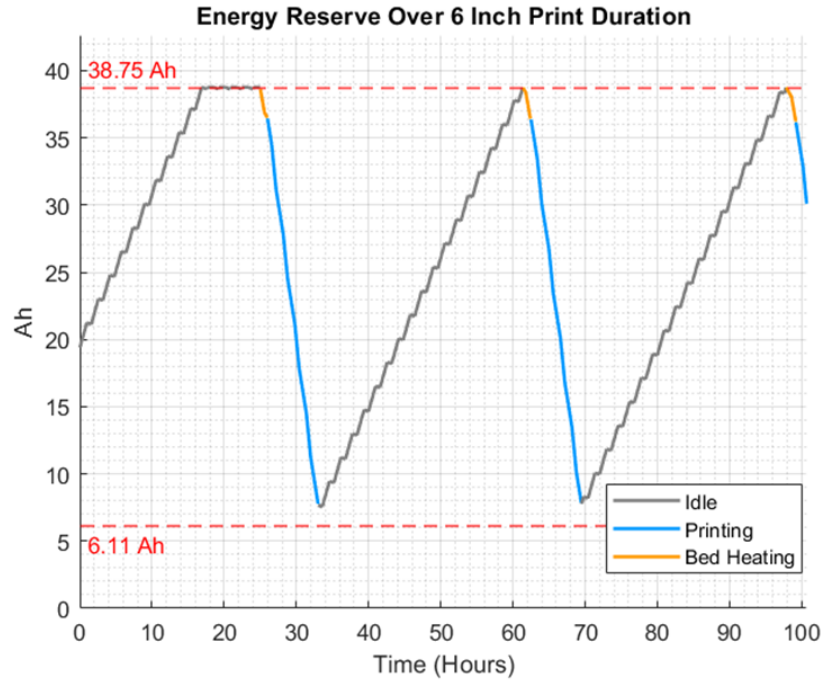


Fig. 9 Full Print Cycle Battery Charge. The power draw of the fabrication subsystem during printing cycles between a charging phase up to 38.75 Ah (80%) battery storage followed by a discharge down to 6.11 Ah (20%) battery storage during voxel deposition. Ridges in the charge cycle are caused by eclipsing from the Earth. The time to print a 6-inch-tall cylinder is estimated to be approximately 100 hours (63 orbits), with the first 24 hours allocated for idle charging.

H. Data Handling

The Command and Data Handling (C&DH) system coordinates all communications between the core computer and payload subsystems, enabling command execution, telemetry acquisition, and autonomous fault response. Data collected by the core computer is stored onboard and can be transmitted to ground through the satellite bus communication system upon request.

1. Core Computer and Data Storage

The onboard core computer was selected by the trade study shown in Appendix E. The power consumption, dimensions, mass, cost, and performance of candidate systems were compared to decide the optimal core computer system. Only radiation hardened, space-rated systems were considered in the trade study. The Sirius OBC LEON3FT was ultimately selected and includes 64 MB RAM and 2 GB NAND Flash memory.

The core computer serves as the central C&DH unit, responsible for interfacing with all payload subsystems, running commands, collecting telemetry, and managing fault handling with integrated FDIR logic.

Figure 10 is a flow chart of the low-level communication and data handling sequence during the deployment and additive manufacturing phases. Each decision node represents either a command acknowledgment or telemetry verification from a subsystem.

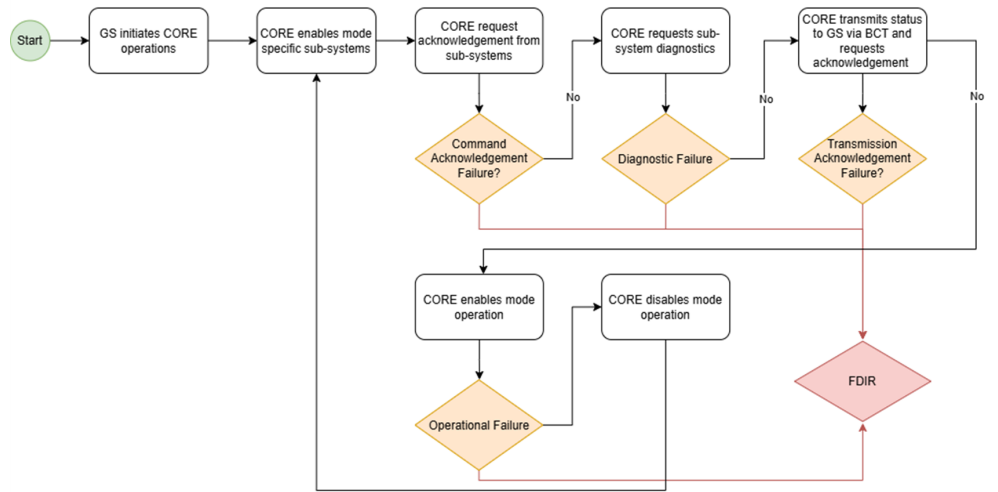


Fig. 10 Low-Level Communication and Data Handling. The initialization system of the payload follows sequential steps to initialize all of the payload systems before beginning the fabrication process. FDIR is engaged in the event that a false condition is returned by any system.

2. Communications Specifications

The payload bus supports an array of different communication antennas. The S- Band All-Metal Patch Antenna was selected from the BCT antenna catalog [15].

The 2024 NASA Small Spacecraft Technology State of the Art was referenced to define a robust communication architecture [41]. Two commercial ground station networks were identified as viable options for this mission. These include Swedish Space Corporation (SSC) and Kongsberg Satellite Services (KSAT) [42, 43]. These providers were selected because of their global coverage, high reliability, and compatibility with S band communication. Both providers operate distributed networks that enable frequent and efficient uplink and downlink sessions with LEO satellites. KSAT was ultimately selected because of its ability to downlink and uplink using S-band communication frequencies.

I. Enabling Systems

1. Thermal Management

The payload has both active and passive cooling for its systems. Two radiators are positioned on the outer shell of payload facing away from the solar panels. The radiators support a passive and active liquid cooling loop. The liquid cooling loop will use Novec 7000 Engineering Fluid [44]. Systems without high heat generation are cooled through the passive cooling loop. Systems that generate higher amounts of heat, such as the laser assembly system and deposition system, are cooled by the active liquid cooling loop.

The Sierra Space Miniature Satellite Energy-Regulating Radiator will be used by the passive cooling loop. It has dimensions of 8.5 x 8.5 inches and can dissipate 12 W of power [45]. The active cooling loop will utilize a custom radiator panel manufactured by Fabrisonic, an ultrasonic additive manufacturing company [46]. The radiator will be ultrasonically additively manufactured with metals designed to provide superior heat dissipation than standard alloys.

III. System Summary

A. Mass Budget

The estimated mass of the payload is 68 kg. This mass estimate includes growth allowances in accordance with the AIAA Mass Properties Control for Space standard [47]. The mass of each subsystem and the total payload mass is provided in Table 8. A full mass budget including all subsystem components is provided in Appendix H.

Table 8 Preliminary Mass Budget. This table shows the current estimates for the mass budget of the planned payload configuration. Percentage growth allowance is calculated in accordance with the ANSI/AIAA Mass Properties Control for Space Standards [47].

Subsystem	Total Basic Mass (kg)	MGA (%)	Total System Mass (kg)
Chassis	16.2	10-30	18.5
Deposition Mechanism	4.4	5-20	8.5
Filament Handling	0.8	15	0.9
Rotating Bed	2.9	5-20	3.1
Laser Assembly	6.8	5-20	7.9
Assembly Mechanism	0.5	5-10	0.6
Avionics	0.4	15	1.0
Health Monitoring	0.6	20	2.3
Substrate	0.5	10	0.9
Thermal Control	5.1	15	7.7
Power Management	3.7	15	13.0
Electrical	2.5	30	3.6
Total System Mass	44.4		68.0

The predicted mass of the payload over time is shown in Appendix I. The maximum allowable mass provided by the Cosmic Capstone Challenge is 70 kg [1], and the absolute mass limit of the BCT X-Sat Venus class bus is 78 kg [15]. In its current configuration the payload has a mass margin of 2.9%.

B. Power Budget

The power budget of the payload is shown in Table 9. The power estimates for each subsystem include a growth allowance derived from the Space Mission Engineering: The New SMAD [48]. The total power draw of each system exceeds the power generation of the spacecraft bus. This problem is mitigated by cycling operation of high power components and charging a large battery bank.

Table 9 Preliminary Power Budget. The power budget for the payload includes the powered subsystems and their power requirements as well as a growth allowance in accordance with the SMAD [48]. The energy a system requires is totaled in kJ based on the amount of time a system is required to run. The system runs power negative while operating many of its subsystems, but proper power cycling allows the system to run with minimal interruption.

Subsystem	Power (W)	Duty Cycle (%)	Growth (%)	Total Power (W)	Time Run (min)	Total (kJ)
Assembly Mechanism	640	5-50	5-20	51.4	47	54
Avionics	22.8	20-100	5-10	19.3	92	256
Deposition Mechanism	373	10-90	2-10	284	83	1263
Health Monitoring	81.0	80-100	2-5	82.5	93	11
Rotating Bed	70.2	80	5	58.9	74	262
Total Draw				1233		1847
Energy Storage						3907
Energy Generated	60	65	0	60	60	432

C. Mission Cost

Cost analysis was done with the NASA Project Cost Estimating Capability (PCEC) [49]. The analysis was done to estimate the cost of development, manufacturing, and operation of Project Daedalus. The cost of Project Daedalus is estimated to be \$50.4 million for the development, production, and launch of the satellite from a top-down program cost

estimate shown in Table 15 in Appendix III.C. This estimate includes the satellite bus cost, payload development cost, and launch cost. The satellite bus is estimated to cost approximately \$20 million. The production, testing, and operation of the payload including staff and communications is estimated to be \$30.4 million. The payload systems are estimated to cost a total of \$715,000 from a bottom-up cost estimate located in Table 16 Appendix G.

D. Risk

Project Daedalus is an experimental proof-of-concept mission with many risks. The identified risks are separated into mission level risks that affect the mission or payload as a whole, and fabrication system risks unique to the payload fabrication system. The most critical risks to the total payload are saturation of the payload bus ADCS system and the potential of a single event effect damaging the critical onboard computers. To mitigate the risk of loss of control in the event that the ADCS system is saturated, the spacecraft may be able to perform maneuvers to de-saturate the control system allowing the mission to continue. The likelihood of a SEE damaging the spacecraft computers can be reduced by applying appropriate shielding to necessary electronic components.

The unique risks associated with the payload fabrication system have high criticality because of the mission dependence on the functions of the fabrication system. Damages to the deposition subsystem in the fabrication system are critical risks but likelihood of these events occurring can be mitigated by proper monitoring and control. A critical risk to the fabrication system is the possibility moving parts in the system cold welding together. If this occurs the entire fabrication system may cease all function. It is important to adhere to the ESA STM-279 standard for materials to lower the risk of materials cold welding together [50].

Project risks are given a unique identifier and organized into risk matrices in Appendix J. Risk levels are defined by a likelihood and consequence of occurrence. These levels are defined in Table 19. Risk matrices for both mission risk and fabrication risk are shown in Figure 15 and Figure 16. Formal risk statements and mitigation strategies for the mission and fabrication system are shown in Table 20 and Table 21 respectively.

IV. Program Timeline

Project Daedalus is currently in the Research and Development phase of its mission. The project follows the SEH 3.0 NASA Program/Project Life Cycle for unmanned robotic missions [51]. The mission timeline for Project Daedalus is shown in Figure 11.

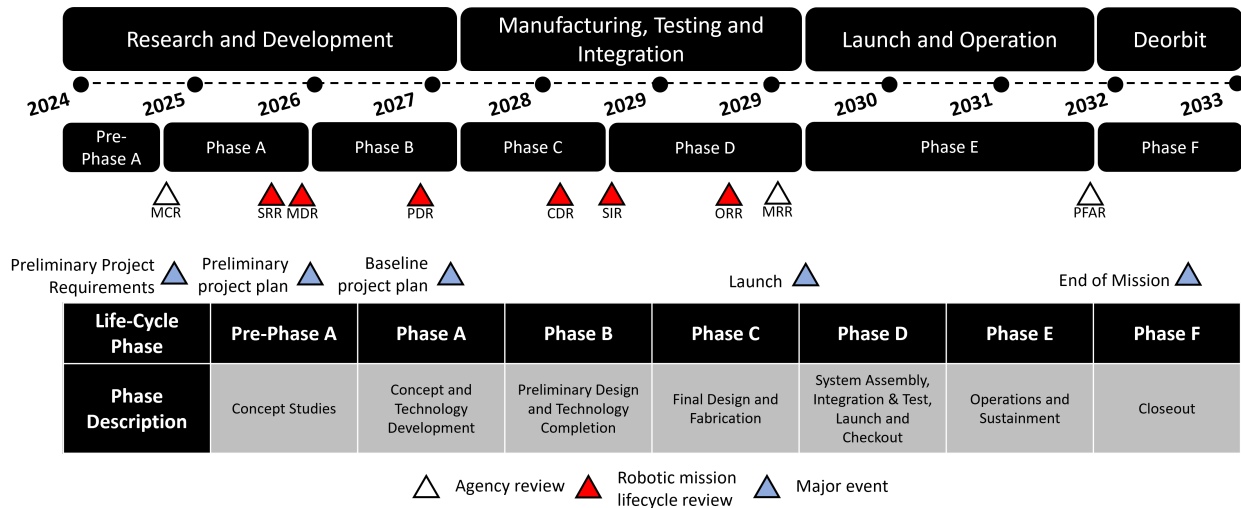


Fig. 11 Project Daedalus Mission Timeline. The timeline for Project Daedalus follows the SEH 3.0 NASA Program/Project Life Cycle structure [51]. Important document deliverables and key mission events are noted on the timeline. The mission is currently planned to launch in 2029 and operate with its end of life planned in 2032. The final end-of-life steps will be taken through the end of 2033.

Project Daedalus is near the end of Phase A of the timeline. The next steps for the mission are to complete the last requirements of Phase A and begin completing objectives for Phase B. The project maturity chart in Appendix K shows

the systems engineering elements that have been completed for Project Daedalus and the elements that still completion for the remaining phases of the project.

V. Summary

Project Daedalus is an experimental mission designed to demonstrate autonomous on-orbit structural assembly and manufacturing. The goal of the mission is to autonomously fabricate several structural cylinders out of aluminum, at which point the payload will weld the cylinders together. Successfully performing the complicated act of additively manufacturing structural elements, manipulating the pieces, and assembling the pieces into a larger structure would mark significant progress in the development of ISAM capabilities. Project Daedalus has an optimistic mission timeline with a launch date in 2029 and an estimated program cost of \$50.4 million. To achieve this goal, research and development through 2027 is necessary to prove all of the technologies shown in this report are ready for the space environment. Development of software and hardware for the advance computers required for the mission is also necessary in this phase. To reach a preliminary design review, all of these steps must be completed. The team is optimistic that the preliminary research performed on the design shown in this paper can inspire a relatively low-cost, high risk, high reward proof of concept mission to further our research in the broad field of in-space assembly and manufacturing.

Acknowledgments

The authors would like to express our gratitude their peer, John Riris for his knowledge on structural theory and help for the project.

The authors would also like to acknowledge and thank Dr. Kevin Shinpaugh and Dr. Randy Spicer for their guidance and support throughout the design of Project Daedalus.

The authors also wish to thank COSMIC, the judges, organizers, and supporters of the COSMIC Capstone Challenge for the opportunity to conceptualize this mission and spacecraft design.

Finally, the authors wish to thank the Kevin T. Crofton Department of Aerospace and Ocean Engineering at Virginia Tech for the opportunity to contribute towards the COSMIC Capstone Challenge and the financial assistance to attend the COSMIC Capstone Challenge final showcase.

References

- [1] “2024 Cosmic Capstone Challenge Information Packet,” , Jan. 2025. URL <https://cosmicspace.org/c3/>, document Number: COSMIC-E01-WD001-2024-B.
- [2] Arney, D., Mulvaney, J., Williams, C., Hernandez, W. A. R., Friz, J., Stockdale, C., Nelson, J., and Vargas, R. R., “In-space Servicing, Assembly, and Manufacturing (ISAM) State of Play - 2024 Edition,” Tech. rep., Oct. 2024. URL <https://ntrs.nasa.gov/citations/20240012414>, nTRS Document ID: 20240012414.
- [3] Gibson, I., Rosen, D., Stucker, B., and Khorasani, M., *Additive Manufacturing Technologies*, Springer International Publishing, Cham, 2021. <https://doi.org/10.1007/978-3-030-56127-7>, URL <https://link.springer.com/10.1007/978-3-030-56127-7>.
- [4] Hsu, K., and Deshpande, A., “Deposition of Solid-Metal Voxels,” , Jan. 2025. URL <https://www.freepatentsonline.com/20250025940.pdf>.
- [5] Hsu, K., “Metal AM Using Vibrational Resonance In-Space via Cold-Welding,” *AIAA SCITECH 2025 Forum*, 2025. <https://doi.org/10.2514/6.2025-1985>, URL <https://arc.aiaa.org/doi/10.2514/6.2025-1985>.
- [6] Deshpande, A., and Hsu, K., “Acoustoplastic metal direct-write: Towards solid aluminum 3D printing in ambient conditions,” *Additive Manufacturing*, Vol. 19, 2018, pp. 73–80. <https://doi.org/10.1016/j.addma.2017.11.006>, URL <https://linkinghub.elsevier.com/retrieve/pii/S2214860417300234>.
- [7] Deshpande, A., and Hsu, K., “The Production of Three-Dimensional Metal Objects Using Oscillatory-Strain-Assisted Fine Wire Shaping and Joining,” *Materials*, Vol. 17, No. 10, 2024, p. 2188. <https://doi.org/10.3390/ma17102188>, URL <https://www.mdpi.com/1996-1944/17/10/2188>.
- [8] Armstrong, M., Mehrabi, H., and Naveed, N., “An overview of modern metal additive manufacturing technology,” *Journal of Manufacturing Processes*, Vol. 84, 2022, pp. 1001–1029. <https://doi.org/10.1016/j.jmapro.2022.10.060>, URL <https://linkinghub.elsevier.com/retrieve/pii/S1526612522007459>.

- [9] Taminger, K. M., and Hafley, R. A., “Electron Beam Freeform Fabrication for Cost Effective Near-Net Shape Manufacturing,” *NATO/RTO AVT-139 Specialists Meeting on Cost Effective Manufacture via Net Shape Processing*, Amsterdam, 2006. URL <https://ntrs.nasa.gov/citations/20080013538>, document ID: 20080013538.
- [10] “ESA launches first metal 3D printer to ISS,” , Jan. 2024. URL https://www.esa.int/Science_Exploration/Human_and_Robotic_Exploration/ESA_launches_first_metal_3D_printer_to_ISS.
- [11] Zocca, A., Lüchtenborg, J., Mühler, T., Wilbig, J., Mohr, G., Villatte, T., Léonard, F., Nolze, G., Sparenberg, M., Melcher, J., Hilgenberg, K., and Günster, J., “Enabling the 3D Printing of Metal Components in μ -Gravity,” *Advanced Materials Technologies*, Vol. 4, No. 10, 2019, p. 1900506. <https://doi.org/10.1002/admt.201900506>, URL <https://onlinelibrary.wiley.com/doi/10.1002/admt.201900506>.
- [12] Zocca, A., Wilbig, J., Waske, A., Günster, J., Widjaja, M. P., Neumann, C., Clozel, M., Meyer, A., Ding, J., Zhou, Z., and Tian, X., “Challenges in the Technology Development for Additive Manufacturing in Space,” *Chinese Journal of Mechanical Engineering: Additive Manufacturing Frontiers*, Vol. 1, No. 1, 2022, p. 100018. <https://doi.org/10.1016/j.cjmeam.2022.100018>, URL <https://www.sciencedirect.com/science/article/pii/S2772665722000083>.
- [13] Rome, J., and Goyal, V. K., “Accelerating Orbital Manufacturing Through In-Space Technology Experiments,” *AIAA SCITECH 2025 Forum*, American Institute of Aeronautics and Astronautics, Orlando, FL, 2025. <https://doi.org/10.2514/6.2025-1981>, URL <https://arc.aiaa.org/doi/10.2514/6.2025-1981>.
- [14] Blue Canyon Technologies, “BCT Product Catalog,” , 2024. URL <https://bluecanyontech.com/static/datasheet/BCT-Product-Catalog.pdf>.
- [15] Blue Canyon Technologies, “NASA RSDO Rapid_BCT Venus Marketing Sheet,” , Mar. 2025. URL https://assets.science.nasa.gov/content/dam/science/cds/spacecraft-development/rsdo/rapid-iv-catalog/NASA%20RSDO%20Rapid_BCT%20Venus%20Marketing%20Sheet_v4.pdf.
- [16] “SpaceX SmallSat Rideshare Program,” , 2025. URL <http://www.spacex.com/rideshare/>.
- [17] “Ansys STK | Digital Mission Engineering Software,” , 2025. URL <https://www.ansys.com/products/missions/ansys-stk>.
- [18] “NEMA23-31-01PD-AMT112S | Stepper Servo Motors,” , 2025. URL <https://www.sameskydevices.com/product/motion-and-control/stepper-servo-motors/nema23-31-01pd-amt112s>.
- [19] “Nema 17 42*48mm 0.35N.m High Low Temp Stepper Motor,” , 2025. URL <http://www.ctrl-motor.com/nema-17-4248mm-035nm-high-low-temp-stepper-motor>.
- [20] “NEMA11-20-02D-AMT112S | Stepper Servo Motors,” , 2025. URL <https://www.sameskydevices.com/product/motion-and-control/stepper-servo-motors/nema11-20-02d-amt112s>.
- [21] Hobbs, K. L., Lyons, J. B., Feather, M. S., Bycroft, B. P., Phillips, S., Simon, M., Harter, M., Costello, K., Gawdiak, Y., and Paine, S., “Space Trusted Autonomy Readiness Levels,” *IEEE Aerospace Conference*, NASA, Big Sky, MT, 2023. URL <https://ntrs.nasa.gov/citations/20220012680>, nTRS Author Affiliations: United States Air Force Research Laboratory, Wright-Patterson Air Force Base, Jet Propulsion Lab, The Aerospace Corporation, Mitre (United States), Katherine Johnson Independent Verification and Validation Facility, National Aeronautics and Space Administration, National Reconnaissance Office NTRS Document ID: 20220012680 NTRS Research Center: Goddard Space Flight Center (GSFC).
- [22] Lanigan, E., “In Situ Process Monitoring: A Perspective on the Role of In Situ Process Monitoring in the Certification of Additive Manufactured Space Hardware,” *Materials Evaluation*, Vol. 80, 2022, pp. 24–27. <https://doi.org/10.32548/2022.me-04261>.
- [23] Holzmond, O., and Li, X., “In situ real time defect detection of 3D printed parts,” *Additive Manufacturing*, Vol. 17, 2017, pp. 135–142. <https://doi.org/https://doi.org/10.1016/j.addma.2017.08.003>, URL <https://www.sciencedirect.com/science/article/pii/S2214860417301100>.
- [24] Muktadir, M., and Yi, S., “Machine Vision-Based Detection of Surface Defects of 3D-Printed Objects,” 2021. <https://doi.org/10.18260/1-2â鉟>.
- [25] El Sallab, A., Sobh, I., Zidan, M., Zahran, M., and Abdelkarim, S., “Yolo4d: A spatio-temporal approach for real-time multi-object detection and classification from lidar point clouds,” 2018. URL https://www.researchgate.net/publication/329245197_YOLO4D_A_Spatio-temporal_Approach_for_Real-time_Multi-object_Detection_and_Classification_from_LiDAR_Point_Clouds.

- [26] Murphy, J., Ward, J. E., and Namee, B. M., “Machine Learning in Space: A Review of Machine Learning Algorithms and Hardware for Space Applications,” *Irish Conference on Artificial Intelligence and Cognitive Science*, 2021. URL <https://api.semanticscholar.org/CorpusID:247477503>.
- [27] Ribani, R., and Marengoni, M., “A Survey of Transfer Learning for Convolutional Neural Networks,” *2019 32nd SIBGRAPI Conference on Graphics, Patterns and Images Tutorials (SIBGRAPI-T)*, IEEE, Rio de Janeiro, Brazil, 2019, pp. 47–57. <https://doi.org/10.1109/SIBGRAPI-T.2019.00010>, URL <https://ieeexplore.ieee.org/document/8920338/>.
- [28] Patil, D. B., Nigam, A., Mohapatra, S., and Nikam, S., “A Deep Learning Approach to Classify and Detect Defects in the Components Manufactured by Laser Directed Energy Deposition Process,” *Machines*, Vol. 11, No. 9, 2023, p. 854. <https://doi.org/10.3390/machines11090854>, URL <https://www.mdpi.com/2075-1702/11/9/854>.
- [29] Yang, C. J., Huang, W.-K., and Lin, K.-P., “Three-Dimensional Printing Quality Inspection Based on Transfer Learning with Convolutional Neural Networks,” *Sensors*, Vol. 23, 2023, p. 491. <https://doi.org/10.3390/s23010491>.
- [30] Arducam, “Arducam 8 MP Sony IMX219 Camera Module,” , 2025. URL <https://www.arducam.com/product/arducam-raspberry-pi-camera-v2-8mp-ixm219-b0103/>.
- [31] Youssef AbouelNour, and Nikhil Gupta, “Assisted defect detection by in-process monitoring of additive manufacturing using optical imaging and infrared thermography,” 2023. URL <https://www.sciencedirect.com/science/article/abs/pii/S2214860423000969#:~:text=Layer-wise%20in-process%20monitoring,as%20point%20and%20line%20defects>.
- [32] Alexander J. Myers a, Guadalupe Quirarte a, Francis Ogoke, Brandon M. Lane, Syed Zia Uddin, Amir Barati Farimani, Jack L. Beuth, and Jonathan A. Malen, “High-resolution melt pool thermal imaging for metals additive manufacturing using the two-color method with a color camera,” 2023. URL <https://www.sciencedirect.com/science/article/pii/S2214860423002762>.
- [33] Teledyne FLIR, “Boson+ Datasheet,” 2025. URL <https://flir.netx.net/file/asset/43192/original/attachment>.
- [34] NASA, “Space Radiation Effects on Electronic Components in Low-Earth Orbit,” , 1999. URL <https://llis.nasa.gov/lesson/824>.
- [35] NOAA, “Solar Cycle Progression | NOAA / NWS Space Weather Prediction Center,” , Apr. 2025. URL <https://www.swpc.noaa.gov/products/solar-cycle-progression>.
- [36] Debra Werner, “Cosmic Shielding works with Aethero to protect Nvidia Jetson Orin NX GPU,” , 2024.
- [37] NASA, “High Performance Spaceflight Computing (HPSC) - NASA,” , 2024. URL <https://www.nasa.gov/game-changing-development-projects/high-performance-spaceflight-computing-hpsc/>.
- [38] Wander, A., and Förstner, R., “Innovative fault detection, isolation and recovery on-board spacecraft: Study and implementation using cognitive automation,” *Conference on Control and Fault-Tolerant Systems, SysTol*, 2013, pp. 336–341. <https://doi.org/10.1109/SysTol.2013.6693950>.
- [39] IMR Batteries, “LG MJ1 18650 3500mAh 10A Battery,” , 2025. URL <https://imrbatteries.com/products/lg-mj1-18650-3500mah-10a-battery>.
- [40] SatSearch, “Starbuck Micro,” , 2025. URL <https://satsearch.co/products/aac-clyde-starbuck-micro>.
- [41] Weston, S. V., Burkhard, C. D., Stupl, J. M., Ticknor, R. L., Yost, B. D., Austin, R. A., Galchenko, P., Newman, L. K., and Soto, L. S., “State-of-the-Art Small Spacecraft Technology,” , Jan. 2025. URL <https://ntrs.nasa.gov/citations/20250000142>, document ID: 20250000142.
- [42] “SSC - Swedish Space Corporation,” , 2025. URL <https://sscspace.com/>.
- [43] “KSAT - Kongsberg Satellite Services,” , Apr. 2025. URL <https://www.ksat.no/>.
- [44] “3M™ Novec™ 7000 Engineered Fluid,” , 2025. URL https://www.3m.com/3M/en_US/p/d/b5005006004/.
- [45] Sierra Space, “Miniature Satellite Energy-Regulating Radiator,” , 2023. URL <https://www.sierraspace.com/wp-content/uploads/2024/01/THERMAL-CONTROL-SYSTEMS-Miniature-Satellite-Energy-Regulating-Radiator-MiSER.pdf>.
- [46] Fabrisonic, “Fabrisonic – 3D Printing Metal with UAM,” , 2025. URL <https://fabrisonic.com/>.
- [47] Beech, G., Adraschko, M., Bautista, J., Cerro, J., Giffiths, W., Herron, J., Holzmann, R., Hundl, R., Lee, B., Kwon, D., Martinez, R., Nakai, J., Plaisted, C., Richbourg, G., Roy, R., Shishko, R., Weitekamp, P., Wolfe, D., and Zimmerman, R., “Mass Properties Control for Space Systems,” , 2015.

- [48] Wertz, J. R., Everett, D. F., and Puschell, J. J. (eds.), *Space mission engineering: the new SMAD*, No. 28 in Space technology library, Microcosm Press, Torrance, 2011.
- [49] “PCEC – Project Cost Estimating Capability - NASA,” , Oct. 2024. URL <https://www.nasa.gov/ocfo/ppc-corner/pcec-project-cost-estimating-capability/>, section: Office of the Chief Financial Officer (OCFO).
- [50] Merstallinger, A., Sales, M., Semerad, E., and Dunn, B. D., “Assessment of Cold Welding Between Separable Contact Surfaces Due to Impact and Fretting under Vacuum,” *ESA Scientific & Technical Memoranda*, Vol. 279, 2009, p. 57. URL <https://ui.adsabs.harvard.edu/abs/2009ESASM.279.....M>, aDS Bibcode: 2009ESASM.279.....M.
- [51] “SEH 3.0 NASA Program/Project Life Cycle - NASA,” , Feb. 2019. URL <https://www.nasa.gov/reference/3-0-nasa-program-project-life-cycle/>.
- [52] “HT08-230 NEMA 8 High Torque Stepper Motor,” , 2025. URL <https://www.applied-motion.com/s/product/nema-08-stepper-motorht08230/01t5i000000y0ZSAAY?name=HT08-230-NEMA-8-High-Torque-Stepper-Motor>.
- [53] Han, S., Park, J., and Kim, J., “Build Plate Heating and Cooling Technique Using Peltier Element for Fused Filament Fabrication,” *Electronics*, Vol. 12, No. 8, 2023, p. 1918. <https://doi.org/10.3390/electronics12081918>, URL <https://www.mdpi.com/2079-9292/12/8/1918>.
- [54] “30-3030 Aluminum Extrusion,” , 2025. URL <https://8020.net/30-3030.html>.
- [55] “MatWeb Online Materials Information Resource - Aluminum 6061-O,” , 2025. URL <https://www.matweb.com/search/DataSheet.aspx?MatGUID=6c41b0bdea564d20b9fd287c03c97923>.
- [56] “McMaster-Carr,” , 2025. URL <https://www.mcmaster.com/>.
- [57] Gutiérrez Arias, G., Jiménez Díaz, F., Rúa Ramírez, E., and Valcarcel Guzman, J., “Thermal Analysis by Finite Elements of Hotends for 3D Printing by Fused Filament Fabrication,” *Periodica Polytechnica Mechanical Engineering*, Vol. 65, No. 2, 2021, pp. 129–133. <https://doi.org/10.3311/PPme.16203>, URL <https://pp.bme.hu/me/article/view/16203>.
- [58] Spicer, R., Miranda, F., Cote, T., Itchkawich, T., and Black, J., “High Vacuum Capable Fused Filament Fabrication 3D Printer, Part II: High-Temperature Polymers Suitable for In-Space Manufacturing,” *Journal of Spacecraft and Rockets*, Vol. 61, No. 2, 2024, pp. 526–542. <https://doi.org/10.2514/1.A35709>, URL <https://arc.aiaa.org/doi/pdf/10.2514/1.A35709?>
- [59] “Online Materials Information Resource - MatWeb,” , 2025. URL <https://www.matweb.com/index.aspx>.
- [60] Hoffmann, M., and Elwany, A., “In-Space Additive Manufacturing: A Review,” *Journal of Manufacturing Science and Engineering*, Vol. 145, No. 2, 2023, p. 020801. <https://doi.org/10.1115/1.4055603>, URL <https://asmedigitalcollection.asme.org/manufacturingscience/article/145/2/020801/1146197/In-Space-Additive-Manufacturing-A-Review>.
- [61] “Inside Electron Beam Welding,” , 2019. URL https://go.additive.ge.com/rs/706-JIU-273/images/GE%20Additive_EBM_White%20paper_FINAL.pdf.
- [62] “Metals - Latent Heat of Melting,” , 2008. URL https://www.engineeringtoolbox.com/fusion-heat-metals-d_1266.html.
- [63] Li, W., Karnati, S., Kriewall, C., Liou, F., Newkirk, J., Brown Taminger, K. M., and Seufzer, W. J., “Fabrication and characterization of a functionally graded material from Ti-6Al-4V to SS316 by laser metal deposition,” *Additive Manufacturing*, Vol. 14, 2017, pp. 95–104. <https://doi.org/10.1016/j.addma.2016.12.006>, URL <https://linkinghub.elsevier.com/retrieve/pii/S2214860416303682>.
- [64] “YLR-150/1500-QCW - IPG Photonics | Laser,” , 2025. URL <https://www.gophotonics.com/products/lasers/ipg-photonics/29-152-ylr-150-1500-qcw>.
- [65] NVIDIA, C., “NVIDIA Jetson Xavier Series,” , 2025. URL <https://www.nvidia.com/en-us/autonomous-machines/embedded-systems/jetson-xavier-series/>.
- [66] Buchner, S., “Radiation Hardness Assurance (RHA) for Space Systems,” *4th International School on the Effects of Radiation on Embedded Systems for Space Applications*, Perot Systems Government Services, Inc., West Palm Beach, FL, USA, 2008. URL https://nepp.nasa.gov/files/25359/SERESSA08_Buchner.pdf.
- [67] VEK, V., “AMD Versal™ AI Edge Series VEK280 Evaluation Kit,” , 2025. URL <https://www.amd.com/en/products/adaptive-socs-and-fpgas/evaluation-boards/vek280.html>.

- [68] AGX, “NVIDIA Jetson AGX Orin,” , 2025. URL <https://www.nvidia.com/en-us/autonomous-machines/embedded-systems/jetson-orin/>.
- [69] AAC Clyde Space, “Sirius OBC LEON3FT,” , 2020. URL https://www.aac-clyde.space/wp-content/uploads/2021/10/AAC_DataSheet_Sirius-OBC.pdf.
- [70] SatSearch, “MA61C CubeSat,” , 2025. URL <https://satsearch.co/products/spin-ma61c>.
- [71] SatNow, “FERMI - Argotec | Satellite On-Board Computer (OBC),” , 2025. URL <https://www.satnow.com/products/on-board-computers/argotec/116-1241-fermi>.
- [72] BAE Systems, “RAD6000 Data Sheet,” , 2006. URL <https://foro.sondasespaciales.com/index.php?action=dlattach;topic=5280.0;attach=334>.
- [73] American Institute of Aeronautics and Astronautics, “Mass Properties Control for Space Systems,” 2015.

Appendix

A. Requirements

Table 10 System Requirements. The full list of mission requirements derived for Project Daedalus are shown below. Requirements involving general space mission and environment considerations were removed from the list in the main body of the paper.

Req ID	Requirement	Source
	The system shall...	
SYS1.0	perform three or more operations to demonstrate an on-orbit ISAM capability.	RFP [1]
SYS2.0	operate autonomously with limited remote commands.	RFP [1]
SYS3.0	meet the BCT X-Sat Venus Class bus specifications.	RFP [1]
SYS4.0	utilize power supplied by the BCT-X Sat Venus class bus.	RFP [1]
SYS5.0	survive launch loads and function in the space environment.	SpaceX [16]
SYS6.0	operate in the space environment.	RFP [1]
SYS7.0	dissipate and manage thermal energy	Mission
SYS8.0	determine accurate position, attitude determination, and precise control maneuvers.	Mission
SYS9.0	launch before 2030.	RFP [1]

B. STK Simulation

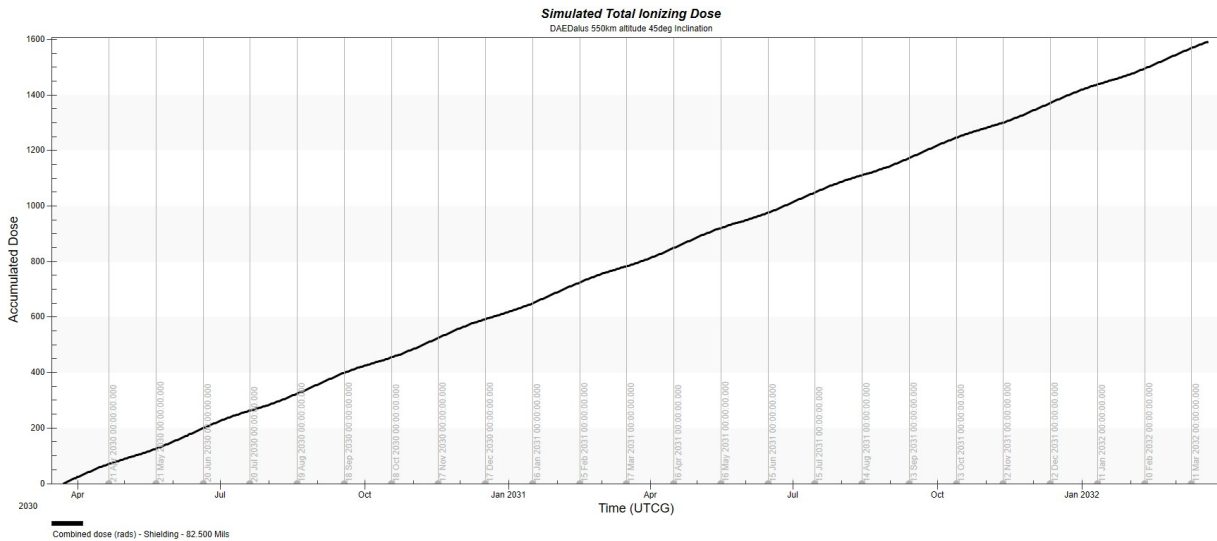


Fig. 12 Daedalus Mission Total Ionizing Dose. The results of an STK simulation for a circular orbit at 550 km altitude and 45° inclination are shown above. This data is the total ionizing dose the satellite experiences over the course of two years assuming it has radiation shielding 2 mm thick.

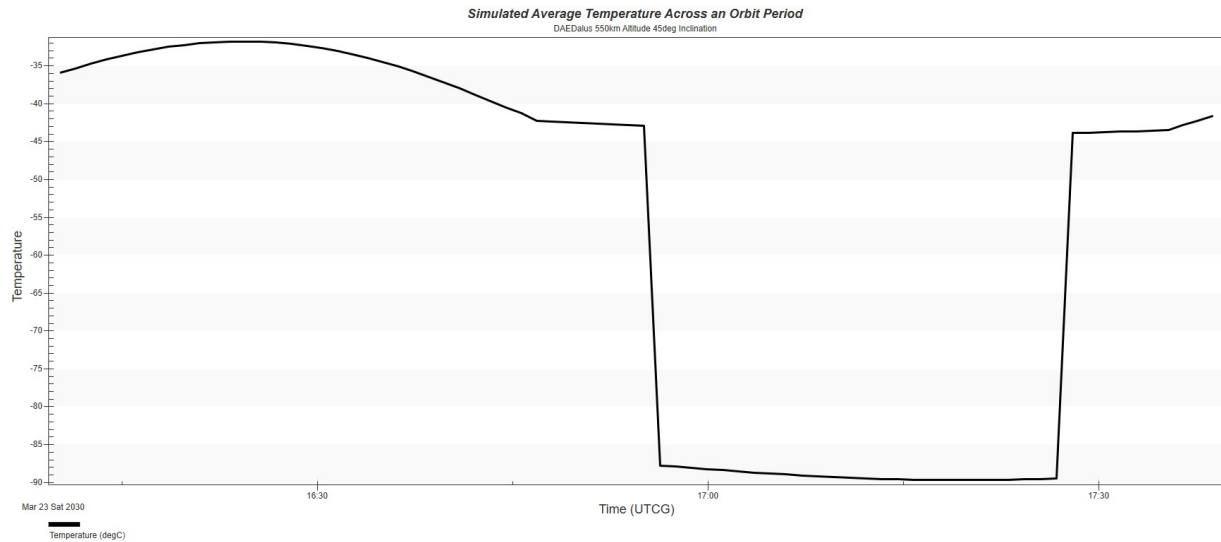


Fig. 13 Daedalus Mission Thermal Cycle. The result of an STK simulation for a circular orbit at 550 and 45° inclination are shown above. This data is the thermal cycle data over the course of a full orbit for the satellite.

C. Additive Manufacturing Trade Studies

Table 11 Additive manufacturing trade study. This table shows the values calculated for each candidate additive manufacturing technique along with the weights given to each value. The final score of each candidate is shown as well. From this trade study, directed acoustic energy deposition was chosen as the additive manufacturing system to be designed for the Daedalus mission.

	Power (W)	Volume (m ³)	Mass (kg)	Research Value	Result	Source
Weights	0.331	0.167	0.148	0.354		
DAED Metal	100 – 300	0.05	20	3	0.36	[4–7, 47, 52–56]
MEX Polymer	150 – 190	0.05	17	1	0.29	[47, 52–60]
EDED Metal	500 – 600	0.06	40	2	0.21	[47, 52–56, 60–62]
LDED Metal	800 – 1000	0.06	40	1	0.14	[10, 47, 52–56, 62–64]

D. AI Computer Trade Study

Table 12 AI Computer Trade Study. The NVIDIA Jetson Xavier NX AI computer was chosen from the trade study in the table below. The figures of merit to determine the optimal AI hardware was power draw (W), dimensions (mm), mass (kg), cost (\$), performance in tera-operations per second (TOPs), and rad hardening (krad).

AI Hardware Model	Power (W)	Dimension (mm)	Mass (kg)	Cost (\$)	Perf. (TOPs)	RHA (krad)	Result	Source
Weights	0.35	0.1	0.2	0.01	0.3	0.04		
NVIDIA Jetson Xavier NX+shield	10W - 20W	70 × 45	0.48	400	21	0.8-1.2	0.273	[65, 66]
AMD Versal VEK280	50W	240.5 x 186.4	0.54	7,000	228	120	0.271	[67]
Nvidia Jetson Orin NX+shield	10W - 30W	100 × 87	0.73	700	157	0.8-1.2	0.262	[66, 68]
NVIDIA Jetson AGX Xavier+shield	10W - 40W	69.6 × 45	0.63	1,000	32	0.8-1.2	0.193	[65, 66]

E. Core Computer Trade Study

Table 13 Core Computer Trade Study. The Sirius OBC LEON3FT was selected based on a trade study assessing power consumption (W), dimensions (mm), mass (kg), cost (\$), and performance (MHz). A weighted decision matrix was used to determine the optimal system for reliable payload-level FDIR capability.

Core Computer	Power (W)	Dimensions (mm)	Mass (kg)	Cost (\$)	Performance (MHz)	Result	Source
Weights	0.25	0.3	0.15	0.05	0.25		
Sirius OBC LEON3FT	1.3	96 × 90 × 17	0.13	50,000	50	0.344	[69]
MA61C CubeSat	1.5	110 × 110 × 35	0.15	200,000	50	0.243	[70]
Argotec FERMI OBC	5.0	102 × 100 × 45	0.5	250,000	100	0.188	[71]
BAE Systems RAD6000	5.0	233 × 160 × 17	1.5	20,000	33	0.125	[72]

F. Detailed Power Budget

Table 14 Detailed Component Power Budget. This power budget includes per-component power, duty cycle, growth, and total energy values. Components are grouped by subsystem. The run time of each subsystem is used to calculate the total amount of energy used by each subsystem.

Subsystem	Component	Power (W)	Duty Cycle (%)	Growth (%)	Total Power (W)	Time Run (min)	Total (kJ)
Assembly Mechanism	Laser chassis	600	5	15	480	5	167
	Linear Actuators	0.01 W/Hz	50	5	0	47	0
	Laser Wobbler	10	10	20	21	10	6
	<i>Total</i>	610	–	–	501	–	173
Avionics	AI Computers	20	80	10	176	75	178
	C&DH Computers	2	100	10	15	93	22
	ADCS	0	100	10	0	93	0
	Radio Board Idle	2	20	5	2	19	2
	Radio Board RX+TX	12	80	5	58	75	54
<i>Total</i>	23	–	–	193	–	255	
Deposition Mechanism	DAED Piezo Transducer (40 kHz)	0	80	10	0	75	0
	Z Actuator Motor	9	80	5	44	75	40
	X Actuator Motor	9	80	5	44	75	40
	Patch Heater Initial	52	10	2	16	10	29
	Patch Heater Maintain	4	90	2	11	84	21
	<i>Total</i>	0	–	–	102	–	129
Health Monitoring	Optical Camera	1	80	5	5	75	14
	Watchdog Timer	0	100	2	0	93	0
	Vibration Sensor	1	100	2	1	93	1
	Temperature Sensor	0	100	2	0	93	0
	Power Sensor	80	100	2	240	93	445
<i>Total</i>	0	–	–	245	–	0	
Rotating Bed	Z Actuator Motor	9	80	5	44	75	40
	Rotational Motor	32	80	5	150	75	139
	Linear Actuators	0.01 W/Hz	80	5	0	75	0
	<i>Total</i>	0	0	0	193	0	0
Total Draw	–	0	–	–	1233	–	556
Energy Storage	Batteries	28	–	–	28	–	206
	Batteries	28	–	–	28	–	412
	<i>Total</i>	–	–	–	56	–	617
Energy Generated	Solar Array	395	65	0	256	60	2844

G. Cost Estimation

Table 15 Top-Down Program Cost Estimate. The top-down cost estimate for Project Daedalus was done using the NASA PCEC cost estimation tool [49]. The estimated cost of Project Daedalus is \$50.4 million including non-recurring and recurring costs.

	Non-Recurring Cost (\$K)	Recurring Cost (\$K)	Total Cost (\$K)
Project Management	800	1,900	2,700
Safety/Mission Assurance	1,200	1,700	2,900
Science/Technology	200	300	500
Payload	200	600	800
Flight Systems	3,200	8,300	11,500
Spacecraft Bus	20,000	0	20,000
Flight System I&T	800	2,300	3,100
Launch Vehicle	1,300	0	1,300
System Integration	400	1,100	1,500
Total	30,000	20,400	50,400

Table 16 Bottom-Up Payload Cost Estimate. The bottom-up cost estimate of the Project Daedalus payload was done by summing estimates of each component cost for the payload together. A growth allowance in accordance with AIAA standards was applied to the basic cost of each subsystem to calculate total cost of the payload [73].

Subsystem	Basic Cost (\$K)	GA (%)	Total Cost (\$K)
Chassis	5.3	10	6.3
Deposition Mechanism	14.1	5-20	15.2
Filament Handling	0.6	15	0.7
Rotating Bed	12.3	5-20	13.0
Laser Assembly	16.0	5-30	19.1
Assembly Mechanism	6.5	5-25	6.9
Avionics	301.5	15	346.7
Health Monitoring	24.6	20	29.6
Substrate	8.5	10	9.30
Thermal Control	100.5	15	115.6
Power Management	130.0	5-15	141.5
Electrical	7.5	45	10.9
Total System Cost	627.4		715.0

Table 17 Detailed Cost Table by Subsystem and Component with Growth Allowance. The cost of each component in the payload subsystems is shown in the table below. This is a more detailed version of the Table 16.

Subsystem	Component	Basic Cost (\$K)	GA (%)	Growth (\$K)	Total Cost (\$K)	Total Subsystem Cost (\$K)
Chassis	Frame	2.3	20	0.45	2.7	6.3
	Shielding	3.0	20	0.60	3.6	
Deposition Mechanism	DAED Piezoelectric Transducer (40 KHz)	0.8	20	0.15	0.9	15.9
	DAED Nozzle	1.4	20	0.27	1.6	
	Z Actuators	6.0	5	0.30	6.3	
	Z Actuator Motor	0.5	5	0.02	0.5	
	X Actuators	4.0	5	0.20	4.2	
	X Actuator Motor	0.3	5	0.02	0.32	
	X-Z Gantry Frame 1	0.3	10	0.03	0.33	
	X-Z Gantry Frame 2	0.3	10	0.03	0.33	
	Nozzle Gantry Frame	0.6	15	0.09	0.69	
	Filament Feedstock	0.1	15	0.01	0.05	
Filament Storage	0.6	15	0.09	0.7		
Rotation Bed	Z Actuator	3.0	5	0.15	3.2	13.0
	Z Actuator Motor	0.2	5	0.01	0.2	
	Rotational Motor	0.1	5	0.01	0.1	
	Bed Frame	0.7	20	0.14	0.8	
	Bed Slewing Ring	0.2	15	0.04	0.3	
	Linear Actuators	8.0	5	0.40	8.4	
Laser Assembly	Laser chassis	15.0	20	3.00	18.0	19.1
	Laser Wobbler	1.0	5	0.05	1.1	
Assembly Mechanism	Bed Frame (including Slewing Ring)	0.5	25	0.1	0.6	6.9
	Linear Actuators	6.0	5	0.30	6.3	
Avionics	AI Computers	1.5	15	0.21	1.7	346.7
	C&DH Computers	300.0	15	45.00	345.0	
Health Monitoring	Optical Camera	1.0	20	0.2	1.2	29.6
	IR Camera	12.4	20	2.5	14.9	
	Watchdog Timer	2.3	20	0.45	2.7	
	Vibration Sensor	2.3	20	0.45	2.7	
	Temperature Sensor	4.5	20	0.90	5.4	
	Power Sensor	2.3	20	0.45	2.7	
Substrate	Substrates	7.2	10	0.72	7.9	9.3
	Substrate Holder	0.4	10	0.04	0.4	
	Substrate Holder Structure	0.9	10	0.01	1.0	
Thermal Control System	Insulation/Shielding	3.0	15	0.45	3.5	115.6
	Radiator Panels	60.0	15	9.00	69.0	
	Active fluid loop	37.5	15	5.62	43.1	
Power Management	PMAD	50.0	15	7.50	57.5	141.5
	Batteries	80.0	5	4.00	84.0	
Electrical	Wiring Harness	7.5	45	3.75	10.9	10.9
Total System Cost		627.4				714.8

H. Mass Budget

Table 18 Detailed Payload Mass Budget. The mass of each component for every payload subsystem is provided in this table. This is a more detailed breakdown of the mass of each system and the growth allowance allotted to each component.

Subsystem	Component	Current Mass (kg)	Num. Req.	GA (%)	Growth (kg)	Total Mass (kg)	Subsystem Mass (kg)
Chassis	Frame	14.2	1	15	2.13	16.33	18.5
	Shielding	2.0	1	10	0.20	2.20	
Deposition Mechanism	Piezoelectric Transducer	0.0	1	20	0.00	0.01	8.5
	Deposition Head	0.1	1	20	0.02	0.12	
	Z Actuators	1.2	2	5	0.06	2.52	
	Z Actuator Motor	0.6	2	5	0.03	1.26	
	X Actuators	1.2	2	5	0.06	2.52	
	X Actuator Motor	0.6	2	5	0.03	1.26	
	X-Z Gantry Frame 1	0.4	1	10	0.04	0.44	
	X-Z Gantry Frame 2	0.2	1	10	0.02	0.22	
Nozzle Gantry Frame	0.1	1	15	0.02	0.15		
Filament Handling	Filament Feedstock	0.3	1	15	0.04	0.29	0.9
	Filament Storage	0.5	1	15	0.08	0.58	
Rotating Bed	Z Actuator	1.2	1	5	0.06	1.26	3.1
	Z Actuator Motor	0.6	1	5	0.03	0.63	
	Rotational Motor	0.3	1	5	0.01	0.26	
	Bed Frame	0.5	1	20	0.10	0.60	
	Bed Slewing Ring	0.3	1	15	0.05	0.35	
	Linear Actuators	0.003	4	5	0.00	0.01	
Laser Assembly	Laser chassis	5.0	1	20	1.00	6.00	7.9
	Laser Wobbler	1.8	1	5	0.09	1.89	
Assembly Mechanism	Bed Frame (including Slewing Ring)	0.5	1	25	0.13	0.63	0.6
	Linear Actuators	0.0	2	5	0.00	0.01	
Avionics	AI Computers	0.3	2	15	0.05	0.69	1.0
	C&DH Computers	0.1	3	15	0.02	0.35	
Health Monitoring	Optical Camera	0.1	5	20	0.02	0.60	2.3
	IR Camera	0.1	2	20	0.02	0.24	
	Watchdog Timer	0.1	3	20	0.02	0.36	
	Vibration Sensor	0.1	3	20	0.02	0.36	
	Temperature Sensor	0.1	3	20	0.02	0.36	
	Power Sensor	0.1	3	20	0.02	0.36	
Substrate	Substrates	0.0	12	10	0.00	0.40	0.9
	Substrate Holder	0.2	1	10	0.02	0.22	
	Substrate Holder Structure	0.3	1	10	0.03	0.33	
Thermal Control System	Insulation/Shielding	2.0	1	15	0.30	2.30	7.7
	Radiator Panels	0.1	12	15	0.02	1.93	
	Active fluid loop	3.0	1	15	0.45	3.45	
Power Management	PMAD	2.5	1	15	0.38	2.88	13.0
	Batteries	1.2	8	5	0.06	10.08	
Electrical	Wiring Harness	2.5	1	45	1.13	3.63	3.6
Total System Mass		44.4					68.0

I. Mass Growth

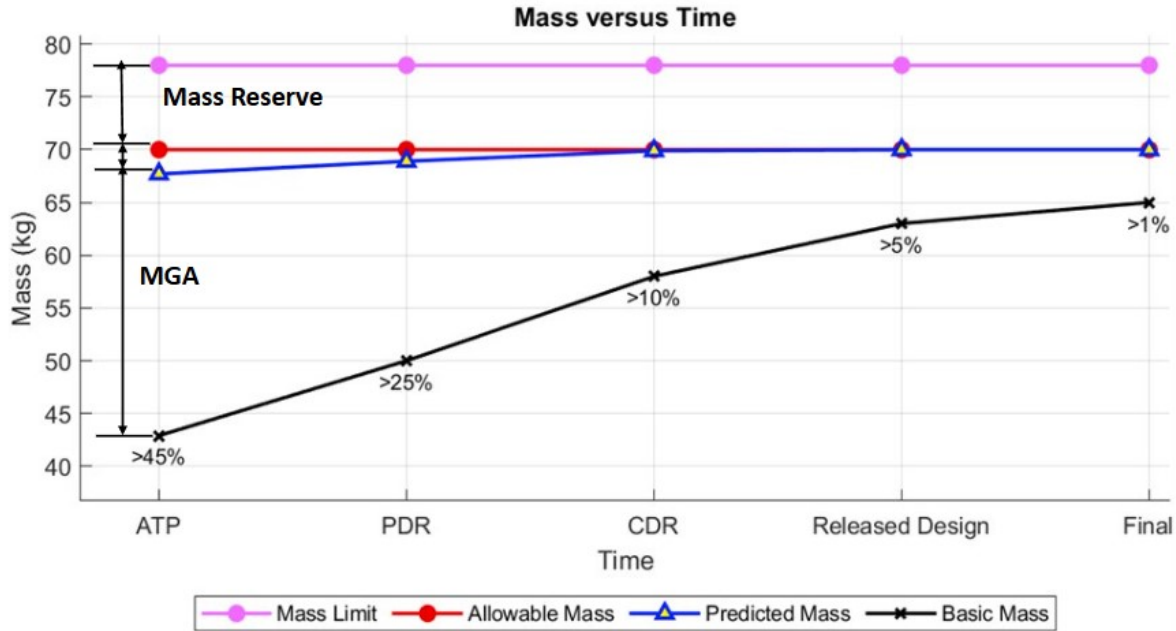


Fig. 14 Mass Budget Timeline. The mass budget for this mission over time through its various development stages is shown above. The mass growth allowance decreases over time as it is filled with mass that was not accounted for in early mass estimates. The Project Daedalus mass budget only has a 2.9% mass margin with the allowable mass of 70 kg provided by the Cosmic Capstone Challenge [1].

J. Risk Analysis

Table 19 Risk Level Definition. Risk is quantified by the likelihood and consequence of an event occurring. The consequence scale and likelihood scale are defined in this table.

Consequence		Likelihood	
Catastrophic (5)	Loss of critical satellite functionality. Satellite is no longer able to operate and can no longer accomplish any mission goals.	Very High (4)	51%–100%
Critical (4)	Loss of satellite functionality. Satellite is no longer able to accomplish some mission goals.	High (4)	26%–50%
Moderate (3)	Impaired satellite functionality. Satellite still effectively operates and can accomplish mission goals but is significantly impaired.	Medium (3)	13%–25%
Minor (2)	Minor impairment to satellite functionality. Satellite can operate and accomplish mission goals but does so with less efficiency or effectiveness.	Low (2)	6%–12%
Negligible (1)	Satellite operates with little issue. Possibility of minor efficiency loss.	Very Low (1)	0%–5%

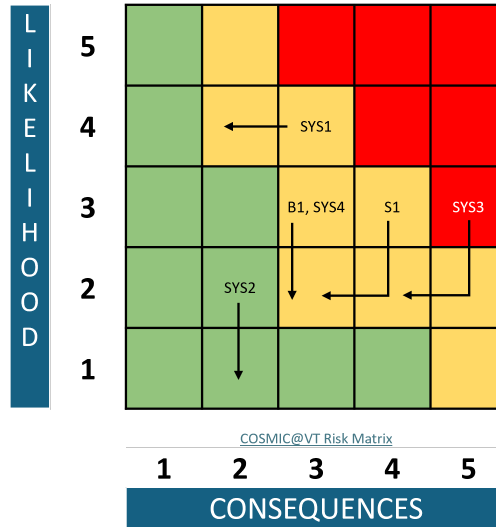


Fig. 15 Mission Risk Matrix. This risk matrix shows the high level mission risks identified for Project Daedalus. The arrows on the matrix indicate the likelihood and consequence trend of a risk after risk mitigation strategies are employed. Risk statements corresponding to the risk identifiers in the matrix are shown in Table 20.

Table 20 Mission Risk Table. This table organizes the high level mission risks for Project Daedalus. The formal risk statement and mitigation strategies are shown for each unique risk identifier.

Risk ID	Risk Statement	Mitigation Strategy
SYS1	If the ADCS system is saturated from internal motion of the payload the spacecraft may lose control of its attitude.	Perform spacecraft maneuvers to de-saturate the control system.
SYS2	If thermal energy is not properly dissipated from components experiencing higher thermal energy, critical components may overheat.	Switch operating states as needed to dissipate thermal energy.
SYS3	If a single event effect occurs to the onboard AI or core payload computer system, the mission may be unable to continue.	Apply appropriate radiation shielding to the core and AI computer(s) onboard the payload. Add redundant core and AI computer systems to prevent loss of mission from SEEs.
SYS4	If the mass of the satellite grows beyond expectation the satellite may not meet the BCT X-Sat Venus class bus mass requirement.	
B1	If the system is not designed following good engineering practices, severe cost overruns could occur.	Perform consistent design reviews and updates to prevent cost overruns from critical design errors.
S1	If the program is not managed correctly, schedule overruns resulting in the failure to launch by the end of the decade could occur.	Perform consistent design reviews and updates to prevent schedule overruns from design mistakes. Plan the mission timeline with appropriate buffer before required launch date to prevent a failure to achieve launch by the end of the decade.

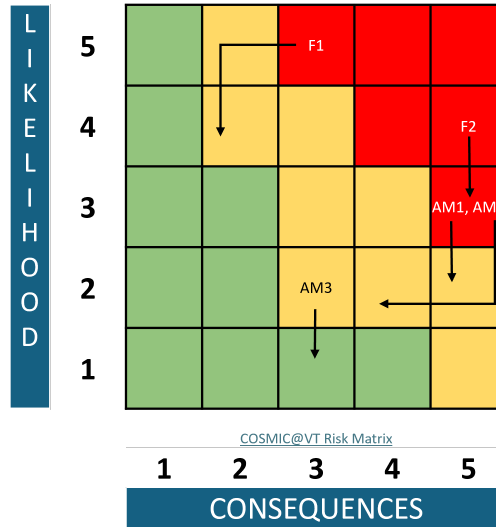


Fig. 16 Fabrication System Risk Matrix. This risk matrix shows the fabrication system risks identified for Project Daedalus. The arrows on the matrix indicate the likelihood and consequence trend of a risk after risk mitigation strategies are employed. Risk statements corresponding to the risk identifiers in the matrix are shown in Table 21.

Table 21 Fabrication System Risk Table. This table organizes the fabrication system risks for Project Daedalus. The formal risk statement and mitigation strategies are shown for each unique risk identifier.

Risk ID	Risk Statement	Mitigation Strategy
F1	If the building component is deformed during the additive manufacturing process the assembly system may be unable to properly assemble the component with another component.	Monitor and actively correct deposition errors with an AI FDIR monitoring system. In the case of a failed print, remove the failed print and substrate to a containment unit.
F2	If moving system components cold weld to other components they contact, parts of the fabrication system may be unable to function which would hinder the mission.	Adhere to ESA STM-279 standard for materials used in system to prevent cold welding.
AM1	If the deposition head is damaged from repeated stress during the additive manufacturing process, the additive manufacturing system may be unable to function resulting in mission failure.	Reinforce deposition head to prevent potential breakage.
AM2	If the aluminum filament is damaged the system may be unable to deposit any material resulting in mission failure.	Utilize a pin roller system to control the speed of spooling into the deposition head; stop feed if necessary. Monitor the filament before spooled into pin roller system.
AM3	If the deposition head is damaged from overheating during the additive manufacturing process, the additive manufacturing system may lose effectiveness, hindering the mission.	Actively monitor the temperature of the deposition head and halt operation as needed.

K. Project Maturity Chart

Product	Mission Phase	Pre-Phase A	Phase A		Phase B	Phase C		Phase D		Phase E	Phase F
	Document	MCR	SRR	MDR/SDR	PDR	CDR	SIR	ORR	FRR	DR	DRR
Stakeholder Identification	Baseline	Update	Update	Update	Update						
Concept Definition	Baseline	Update	Update	Update	Update	Update					
Measure of Effectiveness Definition	Approve	Approve									
Cost/Schedule	Initial	Initial	Update		Update	Update	Update	Update	Update		
SEMP	Preliminary	Baseline	Baseline	Update	Update	Update					
Requirements	Preliminary	Baseline	Update	Update	Update						
Technical Performance Measures			Approve								
Architecture definition			Baseline								
Next level requirements			Baseline								
Required leading indicator trends			Initial	Update	Update	Update					
Design solution definition			Preliminary	Preliminary	Baseline	Update	Update				
Interface definitions			Preliminary	Baseline	Update	Update					
Implementation plans			Preliminary	Baseline	Update						
Integration plans			Preliminary	Baseline	Update	Update					
Verification/Validation plans	Approach		Preliminary	Baseline	Update	Update					
Verification/Validation results						Initial	Preliminary	Baseline			
Operations plans				Baseline	Update	Update	Update				
Operational procedures					Preliminary	Baseline	Update	Update			
Certification (flight/use)							Preliminary	Update			
Decommissioning plans				Preliminary	Preliminary	Preliminary	Update	Update	Update		
Disposal plans				Preliminary	Preliminary	Preliminary	Update	Update	Update	Update	

Fig. 17 Project Daedalus Maturity Chart. This figure shows the systems engineering information required for each phase of the NASA Program/Project Life Cycle structure [51]. Items completed during project development to data are highlighted in blue, items that still require completion are highlighted in orange.